6.1.4 Effect of cooling rate on the microstructure of the final joints

Melt texturing involves slow recombination of the liquid phase with the peritectic Y211 particle to yield the YBCO phase. The recombination process is extremely slow since it is controlled by the dissolution of yttrium in the liquid phase that has a very low solubility limit for yttrium. The peritectic recombination of the Y211 phase with the liquid phase to form YBCO takes place by a nucleation and growth process. Therefore, the cooling rate is expected to have a strong influence on the final microstructure of the samples, grain dimensions and on the superconducting properties. The cooling rate determines the time available for the transport of Y from the Y211 particles to the growing interface.

It has been demonstrated that a high cooling rate causes imperfections on the microstructure of the samples such as: grain boundaries, pores and accumulation of different non-superconducting phases such as Y211 and $BaCuO_2 - CuO$ [76]. At high cooling rates the time available for the peritectic recombination is too small and, then, pores and secondary phases remain. This kind of defects affect the size of the YBCO single domain and, hence, the superconducting properties. On the contrary, decreasing the cooling rate to low values, may cause other problems such as liquid losses, the distortion of the sample geometry and the increase in the processing time.

In this way, a large number of studies have been devoted to the determination of a suitable cooling rate to obtain large YBCO single domains. In our laboratory YBCO single domains have been grown successfully by top seeding melt textured method with a cylindric geometry having a diameter up to 12 mm by using a cooling rate of 0.6°C/h [77]. Moreover, several authors [78, 53] have succeeded in growing single domains with rectangular shape and having dimensions of 40mm×40mm×14mm by using cooling rates between 0.1 and 1°C/h. Efforts have been made to increase the size of the single domain pellets up to 100 mm in diameter [79]. These authors have used a cooling rate of 0.16°C/h. Nevertheless, the growth of such samples can take a very long time (several hundred hours)

and requires a highly controlled process to avoid parasite-grain nucleation.

As an alternative methodology to increase the sample size, research has been focused in developing joining methods. As in the case of YBCO processing, the cooling rate plays an important role in the joining process. Thus, in order to optimize the time of melt processing, on the premise of a perfect crystalline continuity and high superconducting properties, the cooling rate should be investigated. In this way experiments were carried out under the condition of the slow cooling without temperature gradient. For these studies, 10μm Ag foils have been employed, i.e. the thickness which exhibits the best results when the homogeneity of the Ag diffusion was investigated. In our experiments we used as standard a melting time t_{melt}=3 hours and (100)/(100) joints were studied. The thermal profile used in this experiment is shown in figure 6.15. The temperature window ΔT was fixed to ΔT=33°C. Samples of about 1x1x0.6cm^3 were heated

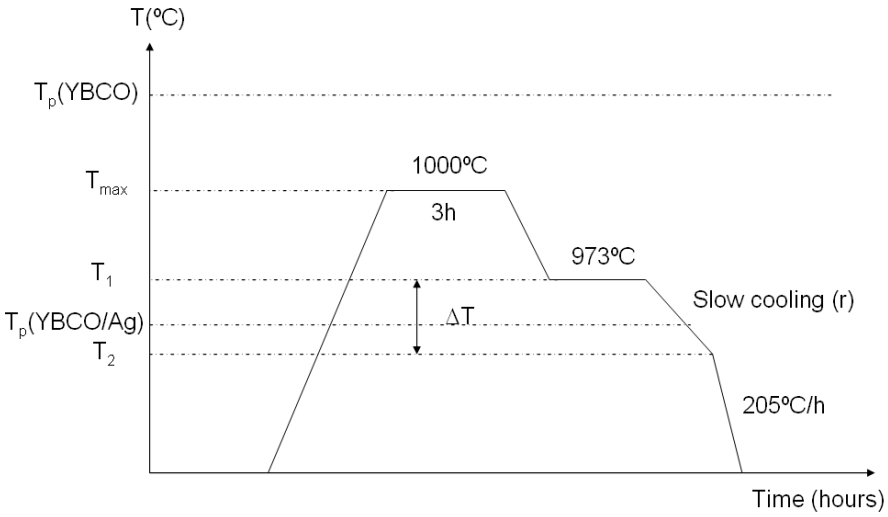

Figure 6.15: Schematic temperature profile used to optimize the cooling rate. The sample is heated up to 1000°C and held at this temperature during 3 hours. This temperature lyes between T_p(YBCO) and T_p(YBCO/Ag). The arrangement is cooled down with different cooling rates of 6, 3, 1.8 and 0.6°C/h in a temperature range of ΔT=33°C.

to the maximum temperature T_{max}=1000°C and held at this temperature for 3

hours to achieve an homogeneous YBCO/Ag interface melting during this time. Ag diffuses into the YBCO matrix up to a certain depth, decreasing the peritectic temperature of the interface. T_{max} is higher than the melting temperature of all that distance closed to the interface, therefore the interface is melted according to the reaction:

$$YBCO + Ag \longrightarrow Y211 + L1 + L2 \tag{6.4}$$

where L1 and L2 designate the Ag-rich and $BaCuO_2$-CuO rich liquids, respectively. Then, the samples were rapidly cooled down to T_1=973°C which is the starting temperature of the slow cooling stage. The slow cooling process has been performed at different rates r (0.6, 1.8, 3 and 6°C/h) down to a temperature T_2=940°C which is lower than the solidification temperature of the YBCO/Ag composite.

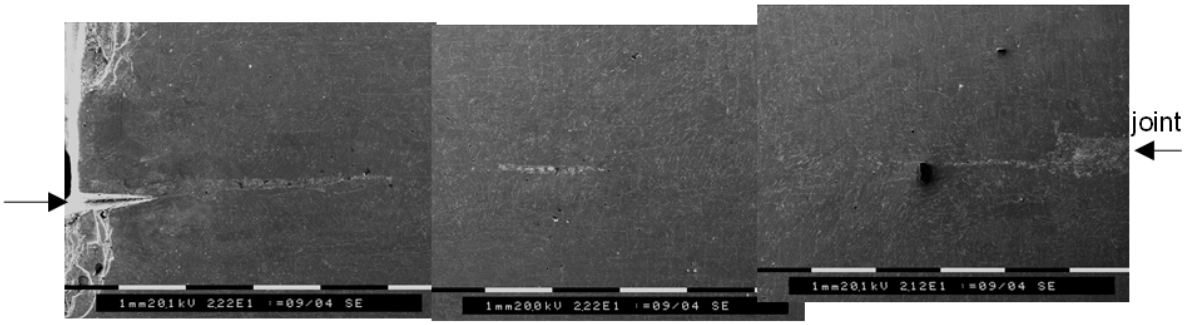

Figure 6.16: General view of the microstructure of the YBCO/Ag/YBCO interface obtained by cooling it down at 6°C/h and obtained by BSE. The junction is indicated by arrows.

The surfaces corresponding to ab planes of all the samples studied in this experiment have been polished in order to observe the quality of the YBCO/Ag/YBCO interface. In figure 6.16 it is shown a general view of the microstructure corresponding to the sample C_6 grown at a cooling rate of 6°C/h. From microstructural observations it is observed that the "good" part of the junction (free of any undesirable phases which can reduce the superconducting

properties of the final joint) corresponds to only $\sim$ 38% of the total length of the junction. Thus, the high quality joint size is considerable reduced. Figures 6.17(a-b) display BSE micrographs showing observations at higher magnification of the final microstructure of the ab plane corresponding to the sample C_6 grown at a cooling rate of 6°C/h. Very different characteristics are observed.

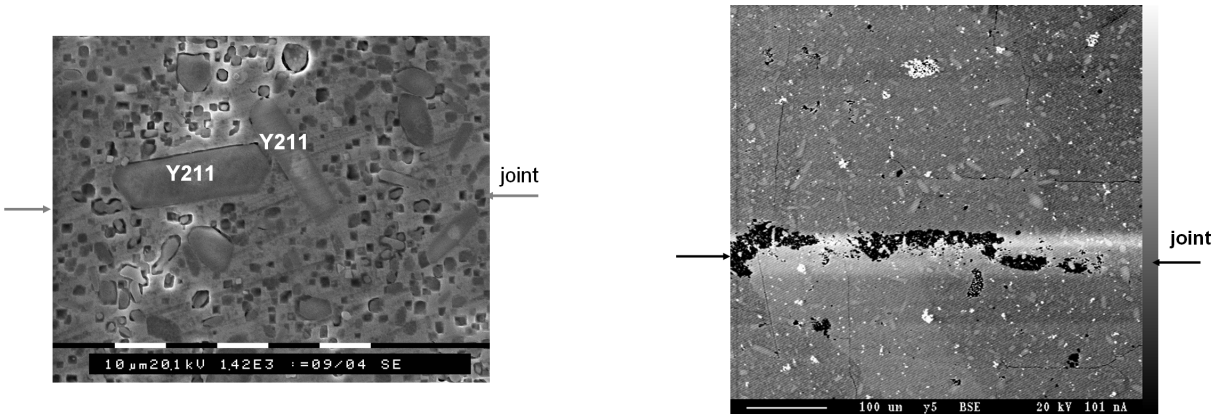

(a) (b)

Figure 6.17: BSE micrographs corresponding to the ab plane of the sample C_6 grown by employing a cooling rate of r=6°C/h. The junction is indicated by arrows. a) BSE micrograph corresponding to the central part of the junction. Some Y211 particles can be observed at the interface; b)BSE micrograph corresponding to the lateral part of the junction where some agglomerations can be observed.

In the first case (figure 6.17a), corresponding to the central part of the junction, it can be observed a perfect matching between both YBCO single domains. Some elongated particles as large as $\simeq$30μm corresponding to the Y211 phase can be observed at the interface, but there is no sign of the junction. In the second case (figure 6.17b), corresponding to the edge of the junction, some degradation can be observed: some segregation of secondary phases remained spread over $\approx$ 72 μm inside the interface while the starting Ag foil was only 10 μm thick. WDS analysis showed that these agglomerates contain Ag and $BaCuO_2$ - CuO phases, the last one resulting from trapping some liquid phase. In figure 6.18a is represented the Ag map where Ag precipitates are the bright particles. In this case we can observe that the Ag precipitates are distributed homoge-

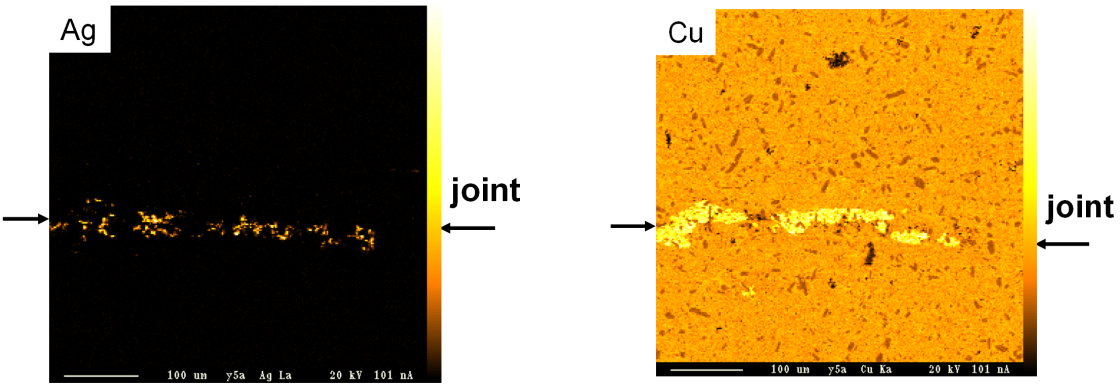

Figure 6.18: Electron microprobe analysis obtained by scanning a 512μm$\times$488μm region corresponding to the edge of the sample C_6 grown by using a cooling rate of r=6°C/h: a) map of Ag-rich region; b) map of Cu-rich region. The junction is indicated by arrows.

neously along the interface. Moreover, Cu map is shown in figure 6.18b showing the same homogeneous dispersion of Cu along the interface. According to these maps of elements, no Ag precipitates and Cu-rich regions can be appreciated inside the YBCO solid matrix. As a consequence, we can state that Ag did not diffuse into the YBCO solid matrix or that the quantity of Ag existing in the YBCO solid is lower than the detection limit of the WDS probe. The first conclusion is much more plausible since the detection limit of the WDS probe is of 0.016%at which is much lower than the solubility of Ag into the YBCO matrix (1-2%at) [80, 81]. This kind of agglomerations reminds particularly the case of the multi-seeded samples [6,7]. The growing fronts have pushed such secondary phases until they meet. Then, these phases have been trapped between the two textured YBCO domains. Unfortunately, such agglomerations are blocking the flow of the superconducting currents and, hence, they decrease the critical current density of the final joint.

By decreasing the cooling rate down to 3°C/h, the microstructure of the joint is improved, as it can be appreciated in the optical micrograph shown in figure 6.19. This figure shows a general view of the interface corresponding to the ab

plane of the sample C_3. Observations at higher magnification of the central part of the junction and of its edge have been performed by SEM microscopy using BSE micrographs (see figures 6.20a and b, respectively). Figure 6.20a shows a section of 170μm$\times$150μm situated at the central part of the junction. Indeed, as in the previous case, a perfect matching is obtained within the YBCO grains. Moreover, some Ostwald ripening of the Y211 particles occurs within the joining area which show some large Y211 particle of $\simeq$30μm. In any case, no additional inclusions of the liquid rich phase BaCuO_2-CuO or Ag are observed. The origin of this Y211 coarsening in the weld region is unknown at present, but it is very likely that it is promoted by the lack of any additive precluding Y211 coarsening, such as Pt [82] or CeO_2 [83].

On the contrary, at the edge of the joint the interface is not clean anymore. A detail of the microstructure which exhibits the joint at its edge is shown in figure 6.20b. On one hand, it can be observed the existence of some impurities, similar to those found in sample C_6. On the other hand, as shown in figure 6.19, the "good" part of the junction free of non-superconducting phases represents $\approx$ 42% from the total length of the junction. The element imaging corresponding to a region of 608μmx580μm situated at the edge of the sample C_3 is shown in figure 6.21. In figure 6.21a the bright zones correspond to Ag precipitates and in figure 6.21b the bright zones indicate the Cu-rich regions. Because of the agglomeration of such phases at the edge of the sample, we conclude that the cooling rate r=3°C/h is still too high and we further followed this investigation by decreasing r.

Figure 6.19: General view of the microstructure of the YBCO/Ag/YBCO interface obtained by cooling it down at 3°C/h and obtained by optical microscopy. The junction is indicated by arrows.

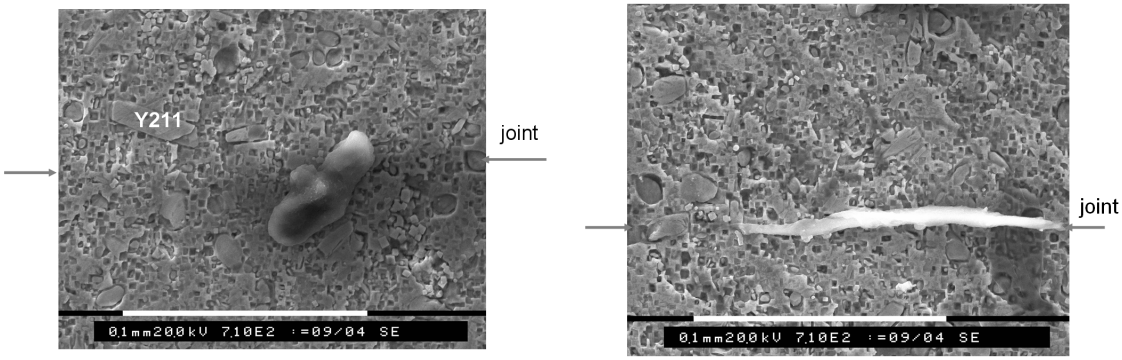

(a) (b)

Figure 6.20: BSE micrographs corresponding to the ab plane of the sample C_3 grown by employing a cooling rate of r=3°C/h. The junction is indicated by arrows. a) BSE micrograph corresponding to the central part of the junction. Some Y211 particles can be observed at the interface; b)BSE micrograph corresponding to the lateral part of the junction where some agglomerations can be observed.

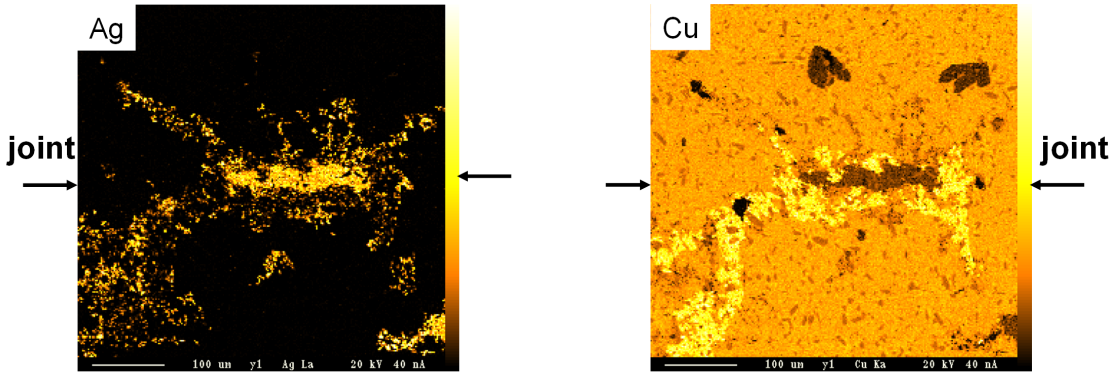

(a) (b)

Figure 6.21: Electron microprobe analysis obtained by scanning a 608μm×580μm region corresponding to the edge of the sample C_3 grown by using a cooling rate of r=3°C/h: a) map of Ag-rich region; b) map of Cu-rich region. The junction is indicated by arrows.

Figure 6.22 shows a general view of the microstructure corresponding to the ab plane of the sample $C_{1.8}$ grown at a cooling rate of 1.8°C/h. The joint is indicated by arrows in the figure. Moreover, note that at the upper right part situated at the edge of the sample, some inhomogeneities can be seen. In this case, the

length joint free of any non-superconducting phases, represents ∼60% from the total length of the junction as it was determined from BSE micrographs. Thus, an improvement occurs when the cooling rate is reduced down to r=1.8°C/h. In this case an inhomogeneous melting zone was created being larger at the end of the joint, this means that Ag has migrated inhomogeneously inside the YBCO solid matrix along the length of the interface.

BSE observations at higher magnification corresponding to the center and the edge of the sample are shown in figures 6.23a and b, respectively. A section of 89μm×71μm from the central part of the junction is shown in the BSE micrograph shown in figure 6.23a. No evidence of the junction is observed, the microstructure of the sample being clean and continuous through the joint. Elongated particles as large as $\sim$ 30μm of Y211 phase can still be observed at the junction. For comparison purposes, in figure 6.24 it is shown a BSE micrograph corresponding to a section of 91μm×72μm situated just below the joint area, in the YBCO matrix, as it is indicated in the scheme at the left hand side of the figure. No large Y211 particles can be seen in the matrix which means that indeed the large Y211 particles found at the interface are formed during the welding process. Note in this figure that the microstructure displays porosity having a square shape and highly visible. This microstructure is the result of chemical etching performed on the samples studied as explained in Chapter 3 in order to obtain a better visualization of the defects existent in the sample.

Evidence of some impurities associated with Y211 phases, Ag precipitates and BaCuO_2-CuO phase can be observed in figure 6.23b. This figure shows a BSE micrograph corresponding to a section of 170μm×140μm located at the edge of the joint. Some porosity is observed too at the edge of the joint corresponding with the YBCO/Ag/YBCO interface. At the interface, besides the porous zone and the molten region existing at the edge of the sample, no secondary phases can be detected anymore at the rest of the junction.

On the contrary, the ab plane of the sample $C_{0.6}$ presents a perfect continuity

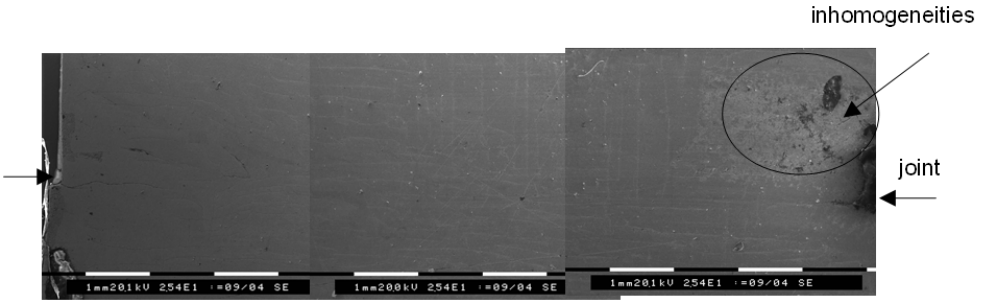

Figure 6.22: General view of the microstructure of the YBCO/Ag/YBCO interface obtained by cooling it down at 1.8°C/h and obtained by SEM. The junction is indicated by arrows.

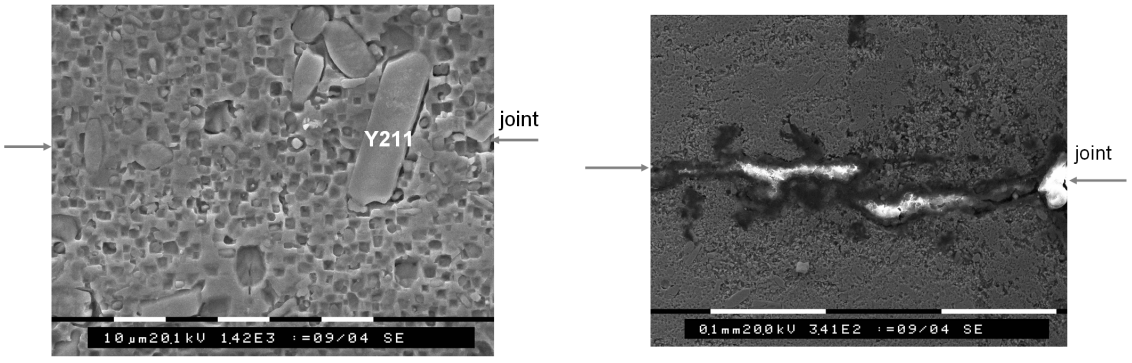

(a) (b)

Figure 6.23: BSE micrographs corresponding to the ab plane of the sample $C_{1.8}$ grown by employing a cooling rate of r=1.8°C/h. The junction is indicated by arrows. a)BSE micrograph corresponding to the central part of the junction. Some Y211 particles can be observed at the interface; b)BSE micrograph corresponding to the lateral part of the junction where some agglomerations can be observed.

across the joint and a clean interface is reached along $\simeq$ 90% of the interface. In figure 6.25 it is shown the microstructure of the ab plane of the YBCO/Ag/YBCO interface all along its length. Thus, no agglomerations like those found in the other samples have been observed in the microstructure of this sample. A higher magnification at the central part of the junction is presented in figure 6.26. There is no sign of the junction and no Y211 particles can be seen at the interface which means that no particle coarsening occurred in this case.

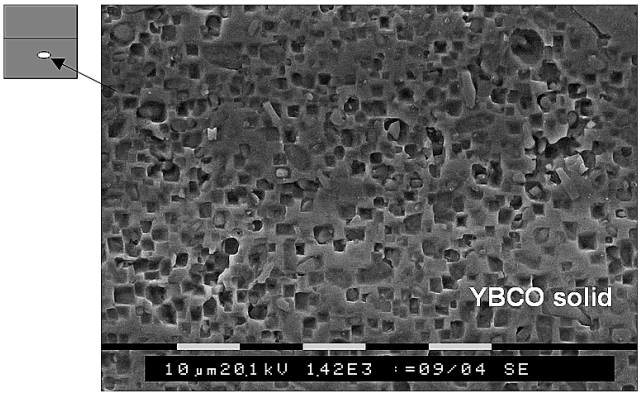

Figure 6.24: BSE micrograph corresponding to a section of 89μm×71μm of the sample $C_{1.8}$ located outside the interface showing the microstructure of the YBCO matrix. In the left part of the figure it is shown by the white circle the region who was analyzed.

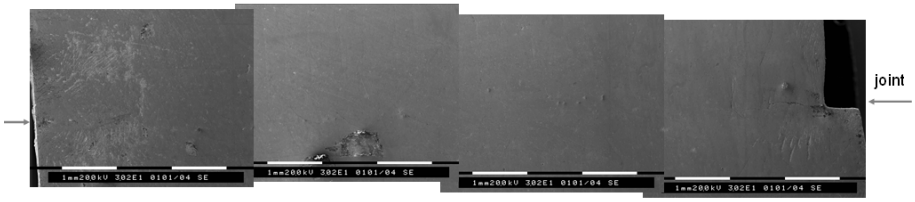

Figure 6.25: BSE micrograph of the joint obtained when the cooling rate is 0.6°C/h. The junction is indicated by arrows.

All the above mentioned results are summarized in figure 6.27 where the variation of the percentage of high quality joint, as a function of the cooling rate, estimated from the SEM and optical micrographs of the polished surfaces, is represented. It can be seen that the size of the high quality joint is reduced with increasing the cooling rate. The size of the high quality joint prepared at a cooling rate of 0.6°C/h is ≈90% from the total size of the sample, while when the cooling rate is 3°C/h only represents ≈ 40% of the joint. The extrapolation of the experimental curve seems to indicate that at r≈0.4°C/h, the high quality joint represents 100% of the total length of the junction, if the sample to be joined has similar dimensions as those studied in this experiment,

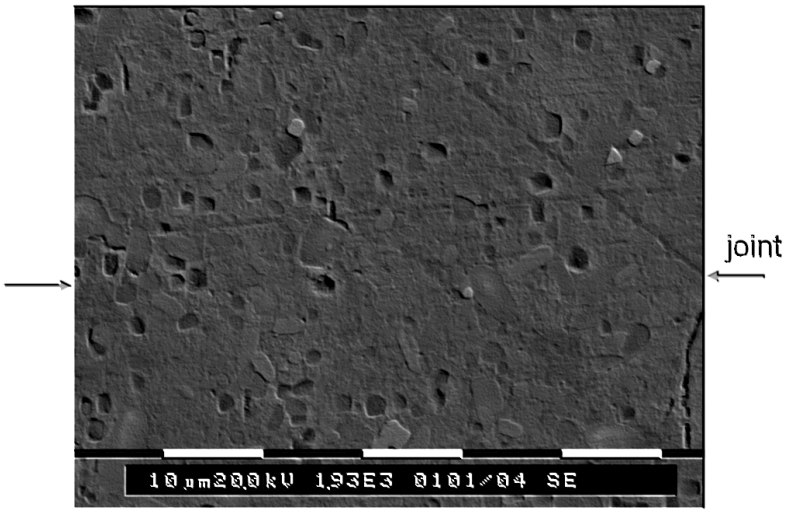

Figure 6.26: BSE micrograph showing a higher magnification of the joint obtained when the cooling rate is 0.6°C/h. The junction is indicated by arrows. No sign of the junction is seen.

i.e. $1\times1\times0.6cm^3$. That means that the slower the cooling rate, the more beneficial for the YBCO/Ag/YBCO interface growth. In addition, the cooling rate being faster than the YBCO/Ag interface growth, could cause some imperfection in the joining area. From our microstructural analysis, we can suggest, then, that Ag precipitates and non-superconducting phases are pushed away from the center of the joining surface towards the edges of the junction where it is expelled from the joining surface.

After this experiment, it is very likely that the crystallization takes place first at the central part of the junction and then the Ag liquid is pushed slowly towards the edges. The accumulation of these phases at the edge of the junction occurs because the cooling rate is too high and the time for the recombination is too low.

The phenomenon of particle pushing by a growing interface is a very general one which was first described by Uhlmann *et al.* [84] (UCJ) for an organic medium with a metallic impurity. Parameters like solidification growth velocity,